TU Delft

Delft University of Technology

Adsorption of n-alkanes in ZIF-8

Influence of crystal size and framework dynamics

Sławek, Andrzej; Roztocki, Kornel; Majda, Dorota; Jaskaniec, Sonia; Vlugt, Thijs J.H.; Makowski, Wacław

DOI
10.1016/j.micromeso.2020.110730

Publication date
2021

Document Version
Accepted author manuscript

Published in
Microporous and Mesoporous Materials

Citation (APA)
Sławek, A., Roztocki, K., Majda, D., Jaskaniec, S., Vlugt, T. J. H., & Makowski, W. (2021). Adsorption of n-alkanes in ZIF-8: Influence of crystal size and framework dynamics. *Microporous and Mesoporous Materials*, *312*, Article 110730. https://doi.org/10.1016/j.micromeso.2020.110730

Important note
To cite this publication, please use the final published version (if applicable).
Please check the document version above.

Copyright
Other than for strictly personal use, it is not permitted to download, forward or distribute the text or part of it, without the consent of the author(s) and/or copyright holder(s), unless the work is under an open content license such as Creative Commons.

Takedown policy
Please contact us and provide details if you believe this document breaches copyrights.
We will remove access to the work immediately and investigate your claim.

This work is downloaded from Delft University of Technology.
For technical reasons the number of authors shown on this cover page is limited to a maximum of 10.

Adsorption of n-alkanes in ZIF-8: influence of crystal size and framework dynamics

Andrzej Sławek,*,† Kornel Roztocki,† Dorota Majda,† Sonia Jaskaniec,‡,¶ Thijs J. H. Vlugt,§ and Wacław Makowski†

†*Jagiellonian University, Faculty of Chemistry, Gronostajowa 2, 30-387 Kraków, Poland*

‡*School of Chemistry, Trinity College Dublin, Ireland*

¶*CRANN&AMBER, Trinity College Dublin, Ireland*

§*Delft University of Technology, Process & Energy Department, Faculty of Mechanical, Maritime and Materials Engineering, Leeghwaterstraat 39, 2628CB Delft, The Netherlands*

E-mail: andrzej.slawek@uj.edu.pl

Abstract

Due to its exceptional chemical and thermal stability, ZIF-8 is one of the most promising representatives of nanoporous metal-organic frameworks. In this work, we investigate adsorption properties of this material both experimentally and theoretically. The experiments were carried out on 8 preparations differing in morphology of the crystals. Adsorption was studied in isothermal approach exploiting standard adsorbates, such as N_2 or CO_2, as well as in isobaric regime with C5–C9 linear alkanes. The latter were performed with the novel quasi-equilibrated temperature-programmed desorption and adsorption (QE-TPDA) technique showing that a complexity of n-alkanes adsorption mechanism in ZIF-8 depends on the nature of adsorbate. Unexpectedly, for adsorption of C7–C9 n-alkanes a two-step process was found. QE-TPDA yielded high quality adsorption isobars which were successfully reproduced by Grand-Canonical

© 2021 Manuscript version made available under CC-BY-NC-ND 4.0 license https://creativecommons.org/licenses/by-nc-nd/4.0/

Monte Carlo molecular simulations. The calculations showed that the specific adsorption behaviour of ZIF-8 is due to the fact that its structure undergoes conformational changes in order to adapt to the guest molecules. QE-TPDA measurements with n-nonane were performed at conditions close to saturation of the adsorbate. This allowed to observe surface-related adsorption on the ZIF-8 crystals, which was correlated with their size.

Introduction

Zeolite imidazolate frameworks (ZIFs) constitute a class of metal-organic frameworks (MOFs), a relatively new and intensively studied family of porous solids.[1,2] ZIFs show exceptional chemical and thermal stability,[3] rarely observed among other types of MOFs,[4,5] which makes them candidates for numerous potential applications in gas separations, catalysis, drug delivery or as sensors.[6–9] One of the most promising zeolite imidazolate frameworks is $[Zn-(mIm)_2 \cdot 2H_2O]_\infty$, better known as ZIF-8, synthesized for the first time in 2006.[10] ZIF-8-based membranes are intensively studied for separation of various gases, including H_2,[11,12] CO_2,[13] or small organic molecules.[14]

The structure of this MOF is formed by Zn^{2+} cations nodes and 2-methylimidazolate (mIm) linkers. These building units create 3-dimensional pore system with a sodalite (SOD) topology comprised of large cavities (diameter of ∼11.7 Å) connected via narrow windows (∼3.4 Å).[15] Moggach et al.[16] found a phase transition of the ZIF-8 framework at high pressures (up to 1.47 GPa) in the presence of a methanol/ethanol mixture. The mIm linkers of ZIF-8 have rotational freedom leading to the change in the size of windows,[17] which is shown in Figure 1. This phenomenon is referred to as "gate-opening" effect.[18] Its occurrence explains the capacity of ZIF-8 to adsorb molecules with higher kinetic diameters than the size of the window such as branched alkanes.[19] To fully understand adsorption of CO_2 and light paraffins in ZIF-8, Fairen-Jimenez et al.[15] simulated adsorption using two rigid forms of this structure. Ania et al.[20] demonstrated more complex adsorption behaviour of this

material by reporting multistep high-resolution adsorption isotherms of N_2, O_2, Ar and CO at cryogenic temperatures, which was explained in detail for Ar by Tanaka et al.[17]

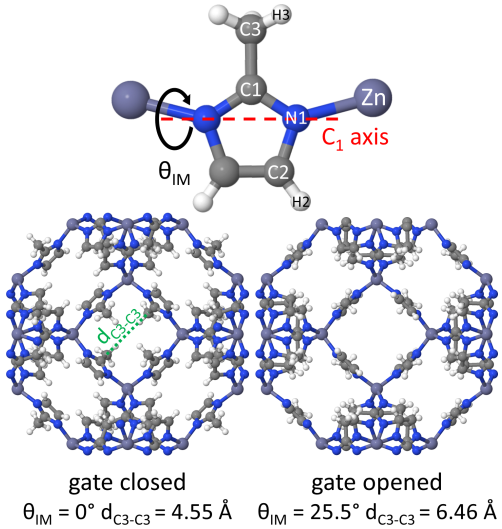

Figure 1: Gate-opening in the ZIF-8 structure: rotation of mIm linkers about an C_1 axis through two N_1 nitrogen atoms resulting in change of the window size.[17] $\Theta_{IM} = 0°$ stands for closed form and $\Theta_{IM} = 25.5°$ for fully opened form.

Thermal stability is a key parameter of MOFs in the context of their potential applications.[4,5] ZIF-8 is known as very stable material, which can withstand temperatures up to 450–550 °C in an inert atmosphere.[3] However, James and Lin[21] showed that the environment is crucial for kinetics of thermal decomposition of this material, as it occurs more rapidly in oxidizing conditions than in inert or reducing ones.

As ZIF-8 arouses a great interest of the scientific community, the preparation methods of this material are well developed.[22] It can be synthesized in high purity through several different synthesis routes with crystal sizes ranging from 50 nm to 300 μm or more.[6,14,23–25] In addition to the standard methods of MOF synthesis based on different treatment of reagent solutions, ZIF-8 can also be obtained in mechanosynthesis, which is found as a cheap and environmentally friendly synthesis method.[26,27] The morphology of microporous solids strongly affects thermodynamics and kinetics of adsorption.[6,12,28–30] However, there are only a few systematic studies regarding the influence of size of the ZIF-8 crystals on these properties. Zhang et al.[31] revealed that structural transition of ZIF-8 upon N_2 adsorption

occurs at a significantly higher pressure in nanoparticles comparing to the bulk phase, which is consistent with the findings of Tanaka et al.[32] showing that crystal downsizing (or high surface-area-to-volume ratio) suppresses the structural flexibility of this MOF.

Quasi-equilibrated temperature programmed desorption and adsorption (QE-TPDA) is a novel experimental technique developed to study adsorption properties of micro- and mesoporous materials.[33,34] The most important feature that distinguishes this method from the conventional ones is the isobaric approach to adsorption measurements. During the QE-TPDA experiments, the pressure is fixed while desorption/adsorption is induced by the change of the temperature of the sample, which allows for faster establishment of adsorption equilibrium and cyclic measurements.[35] In recent years, QE-TPDA was used for several MOFs including MOF-5,[36] Cd-MOF based on 4,4′-sulfonyldibenzoic carboxylate (sdb^{2-}) and 4-pyridinecarboxaldehyde hydrazone (pcih),[37] and STAM-1.[38]

Molecular simulations often serves as a supplementary method helpful in understanding the experimental results on the molecular level or predicting the behaviour of the systems that cannot be directly measured. Monte Carlo (MC) molecular simulations is efficient computational tool often used for modelling the equilibrated adsorbent-adsorbate systems.[39,40] These non-quantum-based calculations rely on force fields to describe the interactions between atoms and molecules. Grand-Canonical Monte Carlo (GCMC) calculations allow to determine average number of guest molecules in the pores of the host structure (loading) at given conditions (T, p), their distribution as well as different energies, including heat of adsorption. One can relate these thermodynamic properties to the microscopic behaviour of the systems, while average loading is directly comparable with experimental adsorption isotherms/isobars. This fact makes GCMC simulations a very attractive computational method for studying adsorption phenomena.

In this work we study adsorption of C5–C9 n-alkanes on crystal-size engineered ZIF-8 with the use of QE-TPDA experimental technique supported by the conventional techniques of measuring porosity, as well as using GCMC molecular simulations.

Materials and methods

Synthesis

All reagents and solvents were of analytical grade (Sigma Aldrich (MERCK), POCH, Polmos) and were used without further purification. The ZIF-8 preparations **(a)**, **(b)**, **(c)**, **(d)**, **(f)**, **(g)**, **(m)** were prepared according to the published methods.[32] However, in case of **(a)**, **(g)**, **(m)**, the synthetic procedures were slightly modified.

ZIF-8 (a): 57.6 mg of Brij® 100 was dissolved in 100 ml of deionized water to prepare a diluted Brij® 100 solution. 0.744 g (2.5 mmol) of zinc nitrate hexahydrate was dissolved in 10 ml of Brij® 100 solution and added to a solution consisting of 12.300 g (0.15 mol) of 2-methylimidazole in 90 ml of Brij® 100 solution. The mixture was stirred at room temperature. The solution "quickly" became cloudy and a suspension was obtained. 24 h later, the suspension was centrifuged and washed with methanol three times. The products were then dried for 24 h under reduced pressure at 40 °C.

ZIF-8 (g): 3.530 g (11.9 mmol) of zinc nitrate hexahydrate was dissolved in 40 ml of methanol and added to a solution consisting of 1.940 g (23.6 mmol) of 2-methylimidazole and 0.807 g (11.9 mmol) of sodium formate in 40 ml of methanol. The mixture was heated at 90 °C for 24 h in a 4 sealed Teflon jar (100 ml). The suspension was filtrated and washed with methanol three times. The products were then dried for 24 h under reduced pressure at 40 °C.

ZIF-8 (m): ILAG (*ion- and liquid-assisted grinding*) reaction was performed at 1 mmol scale,[26] by placing a mixture of solid reactants ZnO (0.080 g) HMeIm (2-methylimidazole; 0.180 g, 10% excess) into a 10 mL agate jar with 200 μL of a grinding liquid EtOH and with 0.010 g of an NH_4NO_3. Two 7 mm diameter agate balls were added to the reaction mixture, and the mixture was then ground for 30 min in a Retsch MM200 grinder mill operating at

20 Hz. Precipitate was washed several times with MeOH and dried 2 h at 40 °C under low pressure.

Physicochemical characteristics

Elemental analysis: the amount of carbon, hydrogen, and nitrogen in the studied samples were determined by conventional microanalysis with CHNS combustion analyzer (Elementar Vario MICRO Cube) equipped with microbalance.

Thermogravimetric analysis: TGA measurements were performed on a STA 409 PC from NETZSCH Company instrument at a heating rate of 10 °C min–1 in a temperature range of 25 – 600 °C (approx. sample weight of 20 mg). The measurements were performed at atmospheric pressure under flowing synthetic air.

Powder X-ray diffraction: PXRD patterns were recorded at room temperature (295 °C) on a Rigaku Miniflex 600 diffractometer with Cu-K α radiation ($\lambda = 1.5418$ Å) in a 2ϑ range from 3° to 45° with a 0.05° step at a scan speed of $2.5^\circ \cdot \mathrm{min}^{-1}$.

Scanning Electron Microscopy: SEM images were acquired using a Zeiss Ultra Plus field-emission microscope equipped with a Gemini®column, working at acceleration voltages in the range of 1–5 keV. Samples were deposited by drop casting on an aluminium holder.

Adsorption measurements

Nitrogen: adsorption isotherms of N_2 were measured at 77 K (liquid nitrogen bath) using Autosorb IQ (Quantachrome) gas sorption analyser. Prior to the measurements the samples were activated under vacuum at 80 °C for 0.5 h (2 °C/min ramp), then at 120 °C (2 °C/min ramp) for 0.5 h and finally at 200 °C for 5 h (5 °C/min ramp).

Carbon dioxide: adsorption isotherms of CO_2 were measured at 195 K (dry ice/isopropanol bath) using BELSORP-max (MicrotracBEL Corp.) apparatus. Prior to these measurements the samples were evacuated at 100 °C for 18–24 h at reduced pressure.

Alkanes: adsorption of C5–C9 n-alkanes was studied with the quasi-equilibrated temperature programmed desorption and adsorption (QE-TPDA) experimental technique. The QE-TPDA instrument is a modified temperature programmed desorption (TPD) setup, which was described in a previous works.[33] Activation of the sample is performed by placing it in a quartz tube in a flow of He, heating it to 300 °C (10 °C/min ramp), and the cooling it down to room temperature. Then, the flow is switched for helium containing small admixture of hydrocarbon ($<$ 1mol%) that starts isothermal adsorption. After stabilization of the TCD signal, signifying the end of adsorption process, desorption/adsorption cycles are measured. Desorption results from heating of the sample, while adsorption from cooling it according to linear temperature programs with 5 and 2 °C/min ramps. In each QE-TPDA experiment, we measured from 5 to 9 repeatable desorption/adsorption cycles, which proves the stability of the studied material. The experimental adsorption isobars were determined by integrating time-dependent QE-TPDA profiles according to the published methods.[46]

Molecular simulations

In this work we used force field-based Monte Carlo computational techniques exploiting force fields to calculate interactions.[39,40] Guest molecules of n-alkanes were described using TraPPE united atom model of Martin and Siepmann[47] that merges the CH_3 and CH_2 groups into single interaction centres – pseudoatoms. Alkanes were modelled as flexible via TraPPE intramolecular potentials for bonds, bends and torsions.[47]

Guest-host interactions were calculated with Lennard-Jones potential, where ε and σ parameters were mixed according to Lorentz–Berthelot combining rules. For adsorbate we used TraPPE force field. For all framework atoms the parameters were taken from DREIDING,[48] except the ones for zinc taken from UFF.[49] Effective potentials were truncated and shifted to zero at 12 Å. Since the molecules on paraffins are non-polar, the Coulomb contribution to total energy has been neglected. A full set of parameters for the L-J potentials for guests and host is available in Table S2 of the Supporting Information.

Adsorption was calculated using Grand Canonical Monte Carlo (μVT ensemble).[39] Each point on the adsorption isobars corresponds to equilibrium adsorbent-adsorbate state, where chemical potential μ, volume V, and temperature T are fixed.

Structures used in this work were treated as rigid.[50] Positions of atoms were taken from the literature.[3,16,41] Crystallography information files (CIFs) are available in the Supporting Information. We used $2 \times 2 \times 2$ unit cells simulation box with periodic boundary conditions applied.[39]

Pore size distributions were calculated geometrically using the method of Gelb and Gubbins.[51] Helium void fractions were calculated with the Widom particle-insertion method. Pore volumes were calculated by multiplying HVF by 10^3 and dividing the result by framework density (in $\mathrm{kg} \cdot \mathrm{m}^{-3}$). All calculations were carried out using open access RASPA 2.0 simulation code.[40,52]

Results and discussion

Characterization of the studied materials

We synthesized a series of ZIF-8 materials with increasing crystal sizes, which were labelled **(a)**–**(g)**. Elemental analysis was performed showing their overall compliance with the stoichiometric chemical composition $ZnC_8H_{10}N_4$. The structure of the materials were confirmed with powder X-Ray diffraction. The patterns and elemental analysis data are available in the Supporting Information (Figure S1, Table S1). Thermogravimetric analysis (TGA) showed that the temperature of degradation of ZIF-8 in air is ca 450 °C, but it was also found this temperature slightly depends on the morphology of the crystals. Material **(a)** that have the smallest crystals shows the highest reactivity, while material **(g)** the with the largest crystals is the most resistant against oxidation, which is shown in Figure S2 of the Supporting Information.

In Figure 2, we show the particle size distributions of the ZIF-8 materials in this study,

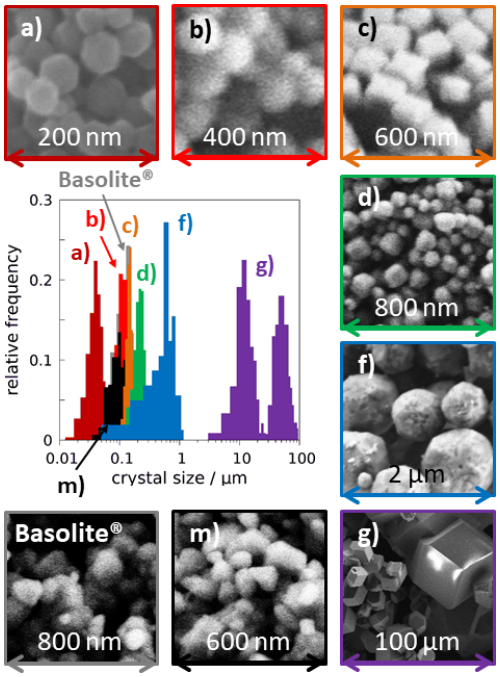

Figure 2: Crystal size distributions of the studied ZIF-8 preparations (labelled **(a)**–**(g)**) estimated based on SEM images.

along with close-ups on SEM images. The size of the crystals ranges from 0.04 µm up to 100 µm. The crystals of preparations **(a)**–**(f)** (0.04–0.6 µm), which were obtained by preticipation from water solution at room temperature, have uniform shape, either cube or chamfered cube (tetratruncated rhombic dodecahedron). Solvothermally synthesized **(g)** crystallized in form of smaller (6–20 µm) and bigger (30–100 µm) rhombic dodecahedrons. Mechanochemically synthesized **(m)** as well as commercial Basolite® Z1200 have crystals of 0.05–0.25 µm with a less defined shape. More detailed information on morphology of each sample can be found in the Supporting Information (Figure S3–S5).

Model of ZIF-8 framework

For molecular modelling, a model of the structure of the studied material is essential. There is a wide selection of ZIF-8 crystal lattice models.[3,16,17,41] In Table 1, we present characteristics of the structures exploited in this work. We used a series of theoretical forms of ZIF-8 structure with the Θ_{IM} angle between linkers (see Figure 1) ranging from -3°to 30°,

Table 1: Characteristics of ZIF-8 structures used in molecular simulations.

	unit cell lengths[a]	window size[b]	cavity size[c]	pore volume[b]
$\Theta_{IM} = -3°$ *		4.34	11.0	0.529
$\Theta_{IM} = 0°$		4.55	11.0	0.523
$\Theta_{IM} = 3°$		4.76	11.0	0.516
$\Theta_{IM} = 6°$		4.98	11.0	0.510
$\Theta_{IM} = 9°$		5.20	11.0	0.505
$\Theta_{IM} = 12°$	16.9856	5.42	10.9	0.500
$\Theta_{IM} = 15°$		5.65	10.8	0.497
$\Theta_{IM} = 18°$		5.88	10.7	0.495
$\Theta_{IM} = 21°$		6.11	10.6	0.498
$\Theta_{IM} = 24°$		6.34	10.5	0.503
$\Theta_{IM} = 27°$		6.58	10.4	0.509
$\Theta_{IM} = 30°$		6.81	10.3	0.514
exp. 1[3]	16.9910	4.51	10.9	0.523
exp. 2[41]	16.8510	4.69	10.9	0.496
exp. 3 LP**[16]	16.9856	4.55	11.0	0.522
exp. 3 HP**[16]	17.0710	6.44	10.5	0.512

** Θ_{IM} from work of Tanaka et al.;[17] ** LP – low pressure; HP – high pressure
[a] in Å; [b] C3-C3 distance in Å; [c] the position of the highest PSD peak in Å; [d] obtained in Monte Carlo simulation using Widom test particle insertion method in $cm^3 \cdot g^{-1}$

where the structure with $\Theta_{IM} = 0°$ is closed (narrow windows), and with $\Theta_{IM} = 25.5°$ is fully opened (wide windows).[17] We compared these structures to the ones obtained experimentally. Structures exp. 1,[3] exp. 2,[41] and exp. 3 LP[16] were solved at atmospheric pressure. They are similar to each other and correspond to the closed form. Exp. 3 HP was obtained at high pressure (1.47 GPa) and corresponds to the opened form.[16] Adsorption-related properties of the studied ZIF-8 models were also designated and analysed. The size of window, defined as C3–C3 distance (Figure 1), varies from 4.34 to 6.81. The size of cavity was obtained from the Monte Carlo calculation of pore size distribution (Figure S13 and S14) slightly varies from 10.3 to 11 Å. Interestingly, the pore volume – determined based on Monte Carlo simulations of Widom particle insertions – is the lowest for ϑ_{IM} angle of ca 18° (Figure S16).

Adsorption

In Figure 3, adsorption isotherms of CO_2 in ZIF-8 materials are shown. For all studied materials we obtained type I CO_2 adsorption isotherms with no hysteresis loops, which are characteristic for microporous materials. Most uptake occurs at relative pressures p/p^0 from 0.05 to 0.1, while sorption capacity ranges from 270 for **(m)** to 290 cm^3-STP·g^{-1} for **(f)**. Apart from the small quantitative differences that may result from measurements uncertainty, the size of crystals does not affect adsorption of CO_2.

Similarly as for CO_2, we found type I adsorption isotherms of N_2 for all studied ZIF-8 preparations (Figure 4), confirming the microporosity of these materials. For N_2 adsorption a small hysteresis loop can be found at relative pressure p/p^0 between 0.05 and 0.3. The loop is narrower and shifted to lower pressures for the materials having larger crystals. This effect is due to structural phase transition depending on the size of the crystals, which was explained in detail in literature.[31,32] In Table 2 we collated values of the micropore volume and specific surface area obtained using the t-plot[42] and Brunauer–Emmett–Teller (BET) methods, respectively. It is important to note that the assumptions of the BET theory are

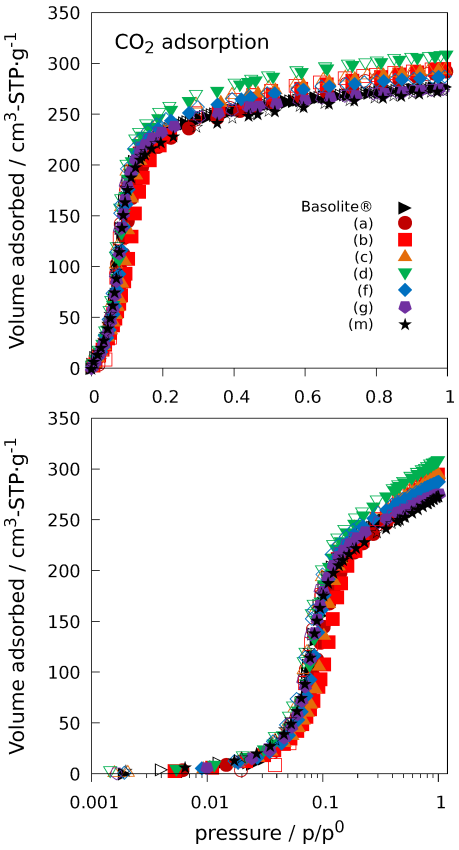

Figure 3: Adsorption isotherms of CO_2 in the studied ZIF-8 at 195 K plotted on linear (top) and logarithmic (bottom) scales. The value of p^0 is ca 1 bar.

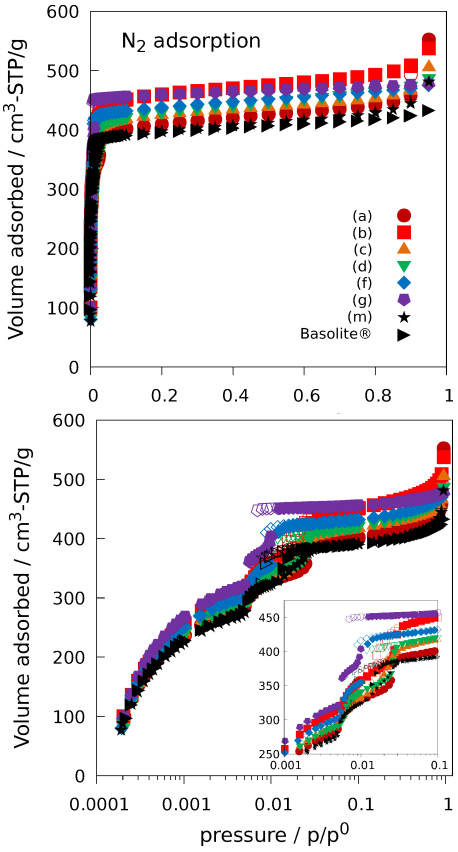

Figure 4: Adsorption isotherms of N_2 in the studied ZIF-8 at 77 K plotted on linear (top) and logarithmic (bottom) scales. The value of p^0 is ca 1 bar.

not met for the microporous materials, especially extremely porous MOFs. However, it is still a commonly used parameter in material chemistry that is associated with porosity. BET specific surface area for the studied ZIF-8 materials ranges from 1636 to 1812 $m^2 \cdot g^{-1}$ (ca 10 %). The volume of micropores that should be independent of the crystal size also varies between 0.526 and 0.630 $cm^3 \cdot g^{-1}$ (ca 16 %), but no trend can be found. The external surface area which is related to the surface of crystallites, is decreasing with increasing size of crystal from ca 200 $m^2 \cdot g^{-1}$ for preparations **(a)** or **(b)** to 61 $m^2 \cdot g^{-1}$ for **(g)**. Detailed information about transformation of N_2 adsorption isotherms and data reduction is available in the Supporting Information (Figure S6, S7, Eq. S3–S10).

Table 2: Characteristics of the porosity of ZIF-8 determined based on N_2 adsorption isotherms measured at 77 K. Crystal sizes determined from SEM images were also included.

	(a)	(b)	(c)	(d)	(f)	(g)	(m)	Basolite®
crystal size[a]	0.040	0.120	0.150	0.220	0.600	5-100	0.220	0.100
micropore volume[b]	0.540	0.604	0.577	0.564	0.609	0.630	0.526	0.537
Surface area (BET)[c]	1636	1800	1876	1654	1812	1734	1699	1772
Surface area (external)[c]	203	208	151	164	87	61	132	97

[a] in μm; [b] in $cm^3 \cdot g^{-1}$; [c] in $m^2 \cdot g^{-1}$

Figure 5a) shows experimental QE-TPDA profiles of n-alkanes in commercial ZIF-8 – Basolite® Z1200, which reflect temperature windows for adsorption and desorption at a given relative pressure of adsorptive. Each profile consist of maxima corresponding to desorption and minima to adsorption. Their intensities are related to momentary amounts of components being desorbed/adsorbed at specific value of temperature. ZIF-8 adsorbs subsequent n-alkanes in the homologous series at increasing temperatures, which results from increasing heats of adsorption. Adsorption of n-pentane (nC5) and n-hexane (nC6) in ZIF-8 is a one–step process, while for C7–C9 n-alkanes two steps might be discerned. For n-heptane (nC7) and n-octane (nC8), both desorption maxima and adsorption minima result from adsorption in bulk (internal micropores) of the ZIF-8 as the relative partial pressures p/p^0 were far from saturation conditions. However, p/p^0 of n-nonane (nC9) was close to 1, thus the low-temperature maxima result from adsorption in the interparticle mesopores or condensa-

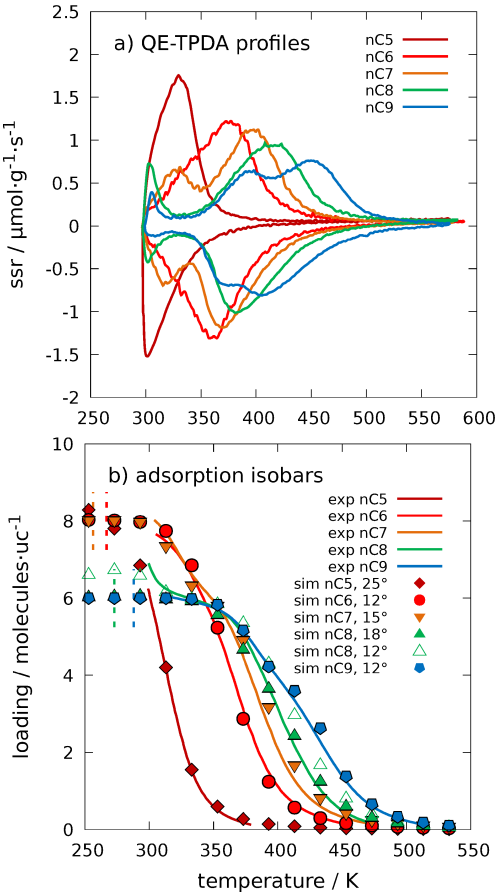

Figure 5: a) QE-TPDA profiles of C5–C9 n-alkanes in the commercial ZIF-8 (Basolite® Z1200). Partial pressures p/p^0 of C5–C9 were ca 0.005, 0.05, 0.08, 0.2, 1, respectively. b) Corresponding adsorption isobars: lines stand for experimental (QE-TPDA) data, while points were calculated with GCMC simulations for structures with different angles between mIm linkers. Vertical dotted lines indicate the condensation temperature of pure adsorbates.

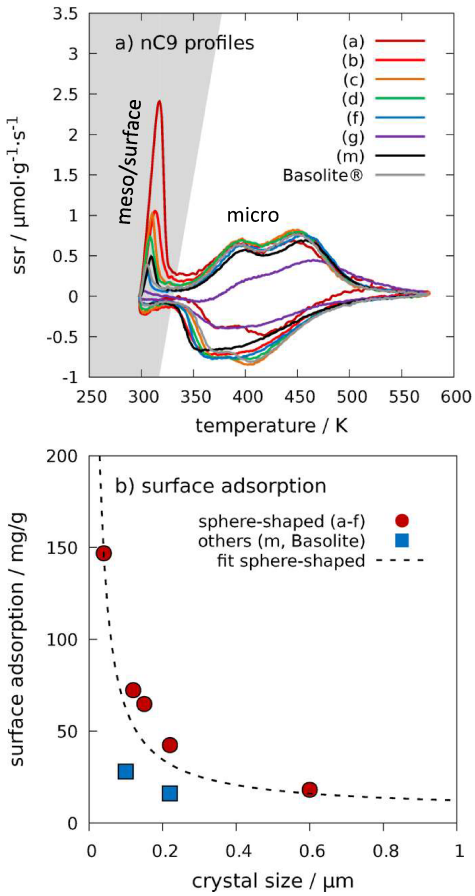

Figure 6: a) QE-TPDA profiles of nonane in the ZIF-8 materials in this study measured at partial pressure p/p^0 close to 1. b) dependence of crystal size on surface area. Dotted line reveals hyperbolic trend.

tion on the external surface of the material, which will be investigated in detail later in this work. Two-step adsorption of nC7 and nC8 in ZIF-8 most likely is the result of framework dynamics of this MOF, in particular arising from rotation of the mIm linkers.

Despite the accuracy and high resolution, QE-TPDA profiles do not provide direct information on the amount of adsorbed components. A quantitative description of the adsorption process is presented by the adsorption isobars in the Figure 5b. It is important to note that a unit cell of the ZIF-8 framework comprises two cavities. Two-step adsorption of nC7, which was clearly observed for the QE-TPDA profiles, is barely marked on the experimental isobar. To fully understand thermodynamics of the adsorption process, we calculated adsorption isobars using Grand Canonical Monte Carlo (GCMC) simulations.[39,40] This computational technique is used to study adsorption equilibrium at static conditions (T, p). More importantly, the values calculated with GCMC technique can be directly compared with the experimental data. Good agreement between experimental lines and calculated points proves accuracy of the exploited theoretical models. The structure of ZIF-8 was modelled with different angles between mIm linkers ranging from -3° to 30° (Figure 1). In Figure 5b we show only the results of calculations most consistent with the experimental data. The full set of data together with average occupation profiles is available in the Supporting Information (Figure S8–S12).

As mentioned before, GCMC simulations reveal thermodynamically favourable equilibrium states of the adsorbent–adsorbate system at given conditions of temperature and pressure. Although the gate-closed ZIF-8 structure ($\mathrm{Ttheta_{IM}} = 0°$) has the smallest cavities (Table 1) effecting in the highest heat of adsorption for all n-alkanes (Figure S15), the values calculated for this form do not coincide with experimental data. In fact, in the presence of C6–C9 n-alkanes, the ZIF-8 structure adopts a transitional form between fully opened and fully closed ($\mathrm{Ttheta_{IM}}$ is between 12 and 18°). Moreover, the molecules of nC5 prefer adsorbing in the opened configuration. It is highly probable that the framework changes continuously with the loading as was reported for adsorption of argon in the literature.[17]

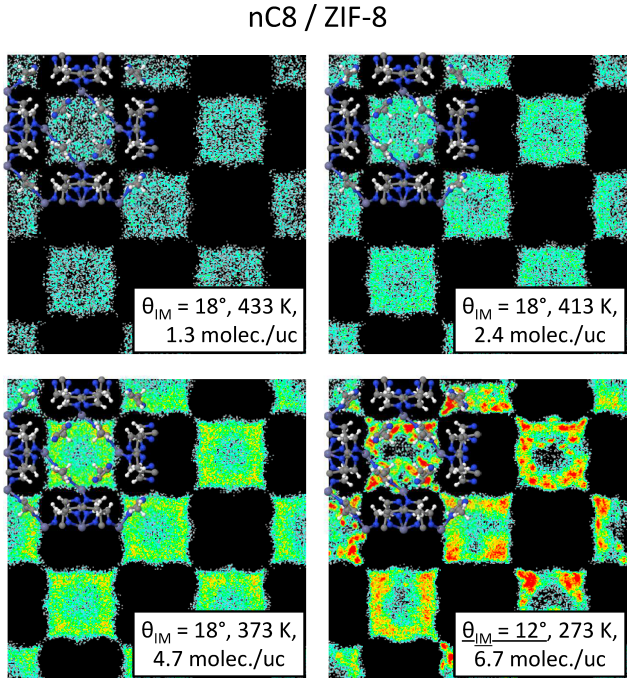

Figure 7: Average occupation profiles of octane in ZIF-8, which were drawn from snaphots corresponding to four points on the GCMC adsorption isobar (Figure 5).

This is clearly seen for adsorption of nC8 in ZIF-8. For loadings lower than 6 molecules per unit cell, the best model that fits to the experimental data assumes Θ_{IM} angle of 18°. Apparently, to adsorb more than 6 molecules per unit cell, the structure needs to change to a more closed form ($\Theta_{\mathrm{IM}} = 12°$) that is able to accommodate up to 8 molecules per unit cell. In Figure 7, we show average occupation profiles of nC8 in ZIF-8 showing preferential situations of the guest molecules in the host structure. Adsorption of n-alkanes in ZIF-8 takes place in the cavities of this material, in a very similar way that we found for LTA-type zeolites.[43] The molecules prefer to locate close to the framework atoms, so the centres of cages are less occupied. Either way, no specific sites for adsorption of C5–C9 n-alkanes can be found in the structures of ZIF-8 (Figure S10–S14), which was confirmed by the analysis of radial distribution functions (Figure S17).

In Figure 6a, the QE-TPDA profiles of nC9 in the studied ZIF-8 preparations are presented. The shape and intensity of these profiles at temperatures above 338 K are similar for all materials except **(a)** and **(g)** and correspond to adsorption in the structural micropores.

For **(a)** the difference is smaller and may result from overall lower porosity of the sample, which was demonstrated by isothermal adsorption measurements of CO_2 or N_2 (Figure 3, 4, Table 2). In the case of preparation **(g)**, most likely, it was not possible to establish equilibrium at used experimental conditions due to kinetic restrictions in large crystals of this material. A smaller amount of sample would be required to be used in the experiment, as well as lower heating/cooling rate and higher carrier gas flow rate. However, results obtained in this way could not be compared with the rest of data. Also, this is insignificant for the further considerations.

The low-temperature parts of the QE-TPDA profiles of nC9 correspond to low-energy adsorption states. Figure 6a shows that for all the studied ZIF-8 materials – except **(g)** – we observe sharp desorption maxima at temperatures below 338 K. We previously reported such peaks for adsorption of nC9 in mesopores of SBA-15 and MCM-41 silicas.[44] They were also observed in the nC9 profiles of fine-crystalline ZSM-5 zeolite[45] and $AlPO_4$ – 5 alumiophosphate.[46] For the investigated ZIF-8 materials the intensity of this low-temperature maxima decreases in the **(a)**–**(f)** series as the size of the crystals increases, which indicate that this effect is correlated with adsorption on the external surface of the ZIF-8 crystals. To obtain the amount of nC9 adsorbed in the micropores and on the surface of crystallites we integrated QE-TPDA maxima in appropriate temperature ranges – 338–550 K and 298–338 K – respectively. The results are collated in Table 3. Adsorption in bulk of the studied ZIF-8 varies between 289.1 and 348.9 $mg \cdot g^{-1}$ (ca 17 %), which is similar deviation to the micropore volume obtained from N_2 adsorption (Table 2). But yet, much more intriguing is the dependence of surface adsorption on the size of crystals which is presented in Figure 6b. For the materials **(a)**–**(f)**, which have roughly uniform distribution of size of crystals (Figure 2), the surface adsorption amount is inversely proportional to the size of the crystals – a hyperbolic trend is observed. This is natural surface-area-to-volume (SA : V) correlation for most of simple solids such as cubes, spheres, tetrahedrons, octahedrons etc.

$$SA : V = \frac{A_1 \cdot a^2}{A_2 \cdot a^3} = A' \cdot \frac{1}{a} \quad (1)$$

where A_1, A_2, A' are the constant coefficients and a is dimension of the particles. Crystals of preparation **(m)** and commercial Basolite® Z1200 are patchy and irregular, so it was difficult to clearly determine their sizes. This can be the reason why we do not find the above-mentioned SA:V relationship for these materials. The QE-TPDA profiles of nC9 on **(g)** were too low to determine adsorption on the surface of this material.

Table 3: Characteristics of the ZIF-8 samples obtained in the QE-TPDA experiments. Crystal sizes determined from SEM images were also included.

	a)	b)	c)	d)	f)	g)	m)	Basolite®
crystal size[a]	0.04	0.12	0.15	0.22	0.6	5–100	0.22	0.1
adsorption (total)[b]	457	383.5	384.5	376.2	367	–	317.1	336.2
adsorption (surface)[b]	146.9	72.3	64.8	42.4	18.1	–	28.0	16.1
adsorption (micro)[b]	310.1	311.1	319.7	333.8	348.9	–	289.1	320.1

[a] in μm; [b] in $mg \cdot g^{-1}$

Conclusions

A wide range of experimental and simulation techniques was exploited to investigate the porosity of ZIF-8 metal-organic frameworks. We synthesized a series of seven ZIF-8 preparations characterized by different morphology of crystals with sizes ranging from nanometre (0.04 μm) to almost millimetre (100 μm). A basic physicochemical characterization of the preparations was carried out. Adsorption measurements of N_2 and CO_2 showed type I adsorption isotherms, revealing that micropore volume and specific surface area do not differ significantly for the studied materials. A t-plot analysis of N_2 adsorption data showed that external surface area is decreasing with increasing size of crystals.

Adsorption of C5–C9 linear alkanes was investigated with quasi-equilibrated temperature programmed desorption and adsorption (QE-TPDA). For n-pentane and n-hexane we observed one-step adsorption that would correspond to the standard adsorption isotherm for

microporous material (type I). C7–C9 n-alkanes exhibit a two-step adsorption behaviour. To obtain a molecular understanding, we reproduced the experimental data with Grand Canonical Monte Carlo (GCMC) molecular simulations. The results of the calculations indicated that the complex adsorption behaviour results from the flexibility of the ZIF-8 framework, as this MOF exhibits gate-opening effect associated with the rotation of the 2-methylimidazolate linkers.[16,17,20] For the adsorption of long, linear paraffins this is manifested by the adaptation of the structure to the guest molecules. It was also shown that the molecules of n-alkanes are located only in ZIF-8 cages, similarly to LTA zeolites.[43]

The QE-TPDA experimental technique was also used to study surface-related adsorption on the ZIF-8. Nanocrystalline ZIF-8 desorbs significant amounts of pre-adsorbed n-nonane at relatively low temperature. This effect is related to the molecules weekly adsorbed on the surface of ZIF-8 crystals. A hyperbolic trend between surface adsorption amount and the size of ZIF-8 crystals was found.

Acknowledgement

This work was supported by the National Science Centre, Poland, grant no. 2016/21/N/ST5/00868. A.S. obtained financial resources as part of financing the doctoral scholarship from the National Science Center, Poland, grant no. 2018/28/T/ST5/00274. T.J.H.V. acknowledges NWO–CW (Chemical Sciences) for a VICI grant. K.R. additionally thanks the National Science Centre (NCN, Poland, Grant no. 2018/28/T/ST5/00333). We are grateful to Prof. D. Matoga for the opportunity to perform syntheses in his laboratory. Prof. H. Tanaka is acknowledged for sending us .cif files for the ZIF-8 structures.

Supporting Information Available

The Supporting Information is available free of charge at ...

Table with chemical composition of the materials under this study obtained with CHNS

elemental analysis. X-Ray diffraction patterns. Results of thermogravimetric analysis: TGA and dTG curves. Scanning electron microscopy (SEM) images of the studied ZIF-8 crystals. Crystal size distribution showed for each preparation. Data reduction exploited for analysis of the adsorption isotherms of nitrogen. Experimental and simulated adsorption isobars of each C5–C9 n-alkanes in the commercial Basolite® Z1200 including calculations performed using different models of ZIF-8 framework – Θ_{IM} dependency. Force fields parameters used in Monte Carlo simulations. Pore size distribution of the studied models of ZIF-8 framework obtained in geometric Monte Carlo calculations. Low-coverage heat of adsorption on C5–C9 n-alkanes calculated using Widom test particle insertion method for ZIF-8 with different Θ_{IM} angle. Dependence of Θ_{IM} angle on theoretical micropore volume.

A crystallography information file (.cif) containing models of ZIF-8 structure with different Θ_{IM} angles (reported by Tanaka et al.[17]) was also included.

References

(1) Zhou, H.-C.; Long, J. R.; Yaghi, O. M. Introduction to Metal–Organic Frameworks. *Chemical Reviews* **2012**, *112*, 673–674, PMID: 22280456.

(2) Zhou, H.-C. J.; Kitagawa, S. Metal–Organic Frameworks (MOFs). *Chem. Soc. Rev.* **2014**, *43*, 5415–5418.

(3) Park, K. S.; Ni, Z.; Côté, A. P.; Choi, J. Y.; Huang, R.; Uribe-Romo, F. J.; Chae, H. K.; O'Keeffe, M.; Yaghi, O. M. Exceptional chemical and thermal stability of zeolitic imidazolate frameworks. *Proceedings of the National Academy of Sciences* **2006**, *103*, 10186–10191.

(4) Bosh, M.; Zhang, M.; Zhou, H.-C. Increasing the Stability of Metal-Organic Frameworks. *Advances in Chemistry* **2014**, *2014*, 8 pages, Article ID 182327.

(5) Yuan, S. et al. Stable Metal–Organic Frameworks: Design, Synthesis, and Applications. *Advanced Materials* **2018**, *30*, 1704303.

(6) Zhang, K.; Lively, R. P.; Zhang, C.; Koros, W. J.; Chance, R. R. Investigating the Intrinsic Ethanol/Water Separation Capability of ZIF-8: An Adsorption and Diffusion Study. *The Journal of Physical Chemistry C* **2013**, *117*, 7214–7225.

(7) Chen, B.; Yang, Z.; Zhu, Y.; Xia, Y. Zeolitic imidazolate framework materials: recent progress in synthesis and applications. *J. Mater. Chem. A* **2014**, *2*, 16811–16831.

(8) Truong, T.; Hoang, T. M.; Nguyen, C. K.; Huynh, Q. T. N.; Phan, N. T. S. Expanding applications of zeolite imidazolate frameworks in catalysis: synthesis of quinazolines using ZIF-67 as an efficient heterogeneous catalyst. *RSC Adv.* **2015**, *5*, 24769–24776.

(9) Kaneti, Y. V.; Dutta, S.; Hossain, M. S. A.; Shiddiky, M. J. A.; Tung, K.-L.; Shieh, F.-K.; Tsung, C.-K.; Wu, K. C.-W.; Yamauchi, Y. Strategies for Improving the Functionality of Zeolitic Imidazolate Frameworks: Tailoring Nanoarchitectures for Functional Applications. *Advanced Materials* **2017**, *29*, 1700213.

(10) Huang, X.-C.; Lin, Y.-Y.; Zhang, J.-P.; Chen, X.-M. Ligand-Directed Strategy for Zeolite-Type Metal–Organic Frameworks: Zinc(II) Imidazolates with Unusual Zeolitic Topologies. *Angewandte Chemie International Edition* **2006**, *45*, 1557–1559.

(11) Xie, Z.; Yang, J.; Wang, J.; Bai, J.; Yin, H.; Yuan, B.; Lu, J.; Zhang, Y.; Zhou, L.; Duan, C. Deposition of chemically modified α-Al2O3 particles for high performance ZIF-8 membrane on a macroporous tube. *Chem. Commun.* **2012**, *48*, 5977–5979.

(12) Zhang, X.; Liu, Y.; Li, S.; Kong, L.; Liu, H.; Li, Y.; Han, W.; Yeung, K. L.; Zhu, W.; Yang, W.; Qiu, J. New Membrane Architecture with High Performance: ZIF-8 Membrane Supported on Vertically Aligned ZnO Nanorods for Gas Permeation and Separation. *Chemistry of Materials* **2014**, *26*, 1975–1981.

(13) Gong, X.; Wang, Y.; Kuang, T. ZIF-8-Based Membranes for Carbon Dioxide Capture and Separation. *ACS Sustainable Chemistry & Engineering* **2017**, *5*, 11204–11214.

(14) Pan, Y.; Lai, Z. Sharp separation of C2/C3 hydrocarbon mixtures by zeolitic imidazolate framework-8 (ZIF-8) membranes synthesized in aqueous solutions. *Chem. Commun.* **2011**, *47*, 10275–10277.

(15) Fairen-Jimenez, D.; Galvelis, R.; Torrisi, A.; Gellan, A. D.; Wharmby, M. T.; Wright, P. A.; Mellot-Draznieks, C.; Düren, t. F., Tina"; swing effect on the adsorption of energy-related gases on ZIF-8: combined experimental,; simulation study, *Dalton Trans.* **2012**, *41*, 10752–10762.

(16) Moggach, S.; Bennett, T.; Cheetham, A. The Effect of Pressure on ZIF-8: Increasing Pore Size with Pressure and the Formation of a High-Pressure Phase at 1.47 GPa. *Angewandte Chemie International Edition* **2009**, *48*, 7087–7089.

(17) Tanaka, H.; Ohsaki, S.; Hiraide, S.; Yamamoto, D.; Watanabe, S.; Miyahara, M. T. Adsorption-Induced Structural Transition of ZIF-8: A Combined Experimental and Simulation Study. *The Journal of Physical Chemistry C* **2014**, *118*, 8445–8454.

(18) Tanaka, D.; Nakagawa, K.; Higuchi, M.; Horike, S.; Kubota, Y.; Kobayashi, T.; Takata, M.; Kitagawa, S. Kinetic Gate-Opening Process in a Flexible Porous Coordination Polymer. *Angewandte Chemie International Edition* **2008**, *47*, 3914–3918.

(19) Ferreira, A. F. P.; Mittelmeijer-Hazeleger, M. C.; Granato, M. A.; Martins, V. F. D.; Rodrigues, A. E.; Rothenberg, G. Sieving di-branched from mono-branched and linear alkanes using ZIF-8: experimental proof and theoretical explanation. *Phys. Chem. Chem. Phys.* **2013**, *15*, 8795–8804.

(20) Ania, C. O.; García-Pérez, E.; Haro, M.; Gutiérrez-Sevillano, J. J.; Valdés-Solís, T.; Parra, J. B.; Calero, S. Understanding Gas-Induced Structural Deformation of ZIF-8. *The Journal of Physical Chemistry Letters* **2012**, *3*, 1159–1164, PMID: 26288051.

(21) James, J. B.; Lin, Y. S. Kinetics of ZIF-8 Thermal Decomposition in Inert, Oxidizing, and Reducing Environments. *The Journal of Physical Chemistry C* **2016**, *120*, 14015–14026.

(22) Lee, Y.-R.; Jang, M.-S.; Cho, H.-Y.; Kwon, H.-J.; Kim, S.; Ahn, W.-S. ZIF-8: A comparison of synthesis methods. *Chemical Engineering Journal* **2015**, *271*, 276 – 280.

(23) Cravillon, J.; Münzer, S.; Lohmeier, S.-J.; Feldhoff, A.; Huber, K.; Wiebcke, M. Rapid Room-Temperature Synthesis and Characterization of Nanocrystals of a Prototypical Zeolitic Imidazolate Framework. *Chemistry of Materials* **2009**, *21*, 1410–1412.

(24) Tanaka, S.; Kida, K.; Okita, M.; Ito, Y.; Miyake, Y. Size-controlled Synthesis of Zeolitic Imidazolate Framework-8 (ZIF-8) Crystals in an Aqueous System at Room Temperature. *Chemistry Letters* **2012**, *41*, 1337–1339.

(25) Kida, K.; Okita, M.; Fujita, K.; Tanaka, S.; Miyake, Y. Formation of high crystalline ZIF-8 in an aqueous solution. *CrystEngComm* **2013**, *15*, 1794–1801.

(26) Beldon, P. J.; Fábián, L.; Stein, R. S.; Thirumurugan, A.; Cheetham, A. K.; Friščić, T. Rapid Room-Temperature Synthesis of Zeolitic Imidazolate Frameworks by Using Mechanochemistry. *Angewandte Chemie International Edition* **2010**, *49*, 9640–9643.

(27) Tanaka, S.; Kida, K.; Nagaoka, T.; Ota, T.; Miyake, Y. Mechanochemical dry conversion of zinc oxide to zeolitic imidazolate framework. *Chem. Commun.* **2013**, *49*, 7884–7886.

(28) Meunier, F. C.; Verboekend, D.; Gilson, J.-P.; Groen, J. C.; Pérez-Ramírez, J. Influence of crystal size and probe molecule on diffusion in hierarchical ZSM-5 zeolites prepared by desilication. *Microporous and Mesoporous Materials* **2012**, *148*, 115 – 121.

(29) Insuwan, W.; Rangsriwatananon, K. Morphology-Controlled Synthesis of Zeolite and Physicochemical Properties. *Engineering Journal* **2012**, *16*, 1–12.

(30) Sakata, Y.; Furukawa, S.; Kondo, M.; Hirai, K.; Horike, N.; Takashima, Y.; Uehara, H.; Louvain, N.; Meilikhov, M.; Tsuruoka, T.; Isoda, S.; Kosaka, W.; Sakata, O.; Kitagawa, S. Shape-Memory Nanopores Induced in Coordination Frameworks by Crystal Downsizing. *Science* **2013**, *339*, 193–196.

(31) Zhang, C.; Gee, J. A.; Sholl, D. S.; Lively, R. P. Crystal-Size-Dependent Structural Transitions in Nanoporous Crystals: Adsorption-Induced Transitions in ZIF-8. *The Journal of Physical Chemistry C* **2014**, *118*, 20727–20733.

(32) Tanaka, S.; Fujita, K.; Miyake, Y.; Miyamoto, M.; Hasegawa, Y.; Makino, T.; Van der Perre, S.; Cousin Saint Remi, J.; Van Assche, T.; Baron, G. V.; Denayer, J. F. M. Adsorption and Diffusion Phenomena in Crystal Size Engineered ZIF-8 MOF. *The Journal of Physical Chemistry C* **2015**, *119*, 28430–28439.

(33) Makowski, W.; Łukasz Ogorzałek, Determination of the adsorption heat of n-hexane and n-heptane on zeolites beta, L, 5A, 13X, Y and ZSM-5 by means of quasi-equilibrated temperature-programmed desorption and adsorption (QE-TPDA). *Thermochimica Acta* **2007**, *465*, 30 – 39.

(34) Makowski, W.; Kuśtrowski, P. Probing pore structure of microporous and mesoporous molecular sieves by quasi-equilibrated temperature programmed desorption and adsorption of n-nonane. *Microporous and Mesoporous Materials* **2007**, *102*, 283 – 289.

(35) Sławek, A.; Vicent-Luna, J. M.; Marszałek, B.; Balestra, S. R. G.; Makowski, W.; Calero, S. Adsorption of n-Alkanes in MFI and MEL: Quasi-Equilibrated Thermodesorption Combined with Molecular Simulations. *The Journal of Physical Chemistry C* **2016**, *120*, 25338–25350.

(36) Makowski, W.; Mańko, M.; Zabierowski, P.; Mlekodaj, K.; Majda, D.; Szklarzewicz, J.; Łasocha, W. Unusual adsorption behavior of volatile hydrocarbons on MOF-5 studied using thermodesorption methods. *Thermochimica Acta* **2014**, *587*, 1 – 10.

(37) Roztocki, K.; Lupa, M.; Sławek, A.; Makowski, W.; Senkovska, I.; Kaskel, S.; Matoga, D. Water-Stable Metal–Organic Framework with Three Hydrogen-Bond Acceptors: Versatile Theoretical and Experimental Insights into Adsorption Ability and Thermo-Hydrolytic Stability. *Inorganic Chemistry* **2018**, *57*, 3287–3296, PMID: 29498839.

(38) Sławek, A.; Vicent-Luna, J. M.; Marszałek, B.; Gil, B.; Morris, R. E.; Makowski, W.; Calero, S. Gate-Opening Mechanism of Hydrophilic–Hydrophobic Metal–Organic Frameworks: Molecular Simulations and Quasi-Equilibrated Desorption. *Chemistry of Materials* **2018**, *30*, 5116–5127.

(39) Frenkel, D.; Smit, B. In *Understanding Molecular Simulation (Second Edition)*, second edition ed.; Frenkel, D., Smit, B., Eds.; Academic Press: San Diego, 2002; pp 1 – 6.

(40) Dubbeldam, D.; Torres-Knoop, A.; Walton, K. S. On the inner workings of Monte Carlo codes. *Molecular Simulation* **2013**, *39*, 1253–1292.

(41) Morris, W.; Stevens, C. J.; Taylor, R. E.; Dybowski, C.; Yaghi, O. M.; Garcia-Garibay, M. A. NMR and X-ray Study Revealing the Rigidity of Zeolitic Imidazolate Frameworks. *The Journal of Physical Chemistry C* **2012**, *116*, 13307–13312.

(42) *Standard Test Method for Determining Micropore Volume and Zeolite Area of a Catalyst*; Standard, 2019.

(43) Sławek, A.; Vicent-Luna, J. M.; Ogorzały, K.; Valencia, S.; Rey, F.; Makowski, W.; Calero, S. Adsorption of Alkanes in Zeolites LTA and FAU: Quasi-Equilibrated Thermodesorption Supported by Molecular Simulations. *The Journal of Physical Chemistry C* **2019**, *123*, 29665–29678.

(44) Mańko, M.; Gil, B.; Janus, R.; Kuśtrowski, P.; Makowski, W. Characterization of the porosity and surface chemistry of mesoporous silicas by quasi-equilibrated thermodesorption of 1-butanol and n-nonane. *Thermochimica Acta* **2010**, *511*, 82 – 88.

(45) Makowski, W.; Mlekodaj, K.; Gil, B.; Roth, W. J.; Marszałek, B.; Kubu, M.; Hudec, P.; Smiešková, A.; Horňáček, M. Application of quasi-equilibrated thermodesorption of linear and di-branched paraffin molecules for detailed porosity characterization of the mono-layered zeolite MCM-56, in comparison with MCM-22 and ZSM-5. *Dalton Trans.* **2014**, *43*, 10574–10583.

(46) Sławek, A.; Vicent-Luna, J. M.; Marszałek, B.; Makowski, W.; Calero, S. Ordering of n-Alkanes Adsorbed in the Micropores of AlPO4-5: A Combined Molecular Simulations and Quasi-Equilibrated Thermodesorption Study. *The Journal of Physical Chemistry C* **2017**, *121*, 25292–25302.

(47) Martin, M. G.; Siepmann, J. I. Transferable Potentials for Phase Equilibria. 1. United-Atom Description of n-Alkanes. *The Journal of Physical Chemistry B* **1998**, *102*, 2569–2577.

(48) Mayo, S. L.; Olafson, B. D.; Goddard, W. A. DREIDING: a generic force field for molecular simulations. *The Journal of Physical Chemistry* **1990**, *94*, 8897–8909.

(49) Rappe, A. K.; Casewit, C. J.; Colwell, K. S.; Goddard, W. A.; Skiff, W. M. UFF, a full periodic table force field for molecular mechanics and molecular dynamics simulations. *Journal of the American Chemical Society* **1992**, *114*, 10024–10035.

(50) Vlugt, T. J. H.; Schenk, M. Influence of Framework Flexibility on the Adsorption Properties of Hydrocarbons in the Zeolite Silicalite. *The Journal of Physical Chemistry B* **2002**, *106*, 12757–12763.

(51) Sarkisov, L.; Harrison, A. Computational structure characterisation tools in application to ordered and disordered porous materials. *Molecular Simulation* **2011**, *37*, 1248–1257.

(52) Dubbeldam, D.; Calero, S.; Ellis, D. E.; Snurr, R. Q. RASPA: molecular simulation software for adsorption and diffusion in flexible nanoporous materials. *Molecular Simulation* **2016**, *42*, 81–101.